Cuadrado, M., Pernas-Sánchez, J., Artero-Guerrero, J. & Varas, D. (2020). Model updating of uncertain parameters of carbon/epoxy composite plates using digital image correlation for full-field vibration measurement. *Measurement, 159*, 107783.

DOI: 10.1016/j.measurement.2020.107783

Model updating of uncertain parameters of carbon/epoxy composite plates using digital image correlation for full-field vibration measurement

M. Cuadrado[a,*], J. Pernas-Sánchez[a], J.A. Artero-Guerrero[a], D. Varas[a]

[a]*Department of Continuum Mechanics and Structural Analysis. University Carlos III of Madrid. Avda. de la Universidad, 30. 28911 Leganés, Madrid, Spain*

Abstract

Model updating is usually based on the contrast between the modal characteristics predicted by the models and those experimentally identified. Traditional experimental methods are based on the use of contacting sensors, but more recently other techniques as 3D Digital Image Correlation have also been used successfully. In this paper the results obtained by applying these alternative techniques are compared, to obtain physically-sound models of carbon/epoxy composite plates. Primarily a roving hammer exciting the plates at evenly distributed degrees of freedom (DoF), and a mono-axial accelerometer attached to a single DoF reference point, have been used for modal identification. Alternatively, high speed cameras were applied to measure full-field vibrations of the plates. 3D DIC allowed obtaining a lower number of natural frequencies but much smoother mode shapes and similar results for model updating. The experimental setup has been benchmarked using two different sets of plates varying thickness and ply stacking.

Keywords: Model updating; Experimental modal data; Digital image

*corresponding author: M. Cuadrado (sanguino@ing.uc3m.es)

1. Introduction

The use of composite laminates is increasing continuously, especially in weight sensitive applications in advanced structural engineering. It can be said that composite materials represent a revolution for aeronautical industry since their application allows to design lighter aircraft with enhanced performance. This leads to a growing need of development of new low-cost, low-time-consuming and effective techniques of evaluation of the performance of the different structural elements constructed with this kind of materials. Particularly, research in composite flat plates used as structural elements for airframes is of major interest. As part of these evaluation methods, numerical models of the structures have been broadly used. The main goal is to have a model that can simulate the structural behaviour of a set of structural components based on their averaged initial characteristics. However, it is important to bear in mind that a model based on the theoretical characteristics of the structure, even though provides useful information, cannot predict its response with a high level of accuracy, due to some uncertainties about its mechanical properties. In the case of composite materials, tests performed on two specimens of the same structural model can display very different dynamic behaviour due to large uncertainties associated with composite material properties or pre-existing imperfections [1]. More specifically, in the case of fiber reinforced plastics (FRP) composite plates, elastic parameters, as the fiber and matrix elastic properties, can differ significantly from those specified by the manufacturers. Additionally, production methods can

introduce some uncertainty about some parameters, as the thickness of the plates (both, mean value and uniformity) or final density. To overcome this problem, theoretical structural models are updated using experimental data of the structural response. Among other methods, non destructive testing as vibration-based techniques, relying on the use of modal data (natural frequencies and mode shapes) obtained experimentally, have been used in civil engineering during the last three decades [2–4], but also more recently for composite plates [5–8]. Traditional experimental modal analysis is based on the use of individual contacting sensors, such as accelerometer, geophones, strain gauges or displacement transducers, which measure only at a set of points of the structures. In the case of thin composite laminates, due to the element's low mass, the total number of sensors must be limited to restrict the added weight, that could affect the results. Thus, in order to obtain accurate modal characteristics, especially in the case of mode shapes, it will be necessary to use whether roving measurement or roving excitation, which will need a high measurement time. More recently other techniques that do not affect the dynamic characteristics of the tested structure have been applied. These techniques can be based on point measures, such as laser vibrometers, but also full-field techniques, such as scanning laser Doppler vibrometers (SLDV) or electronic speckle pattern interferometry (ESPI), can be employed [9]. Full-field techniques are more desirable than single-point ones because they cover the whole area to be analysed. High-speed Digital Image Correlation (DIC) is another one of these full-field techniques that have been successfully used in the field of light plates [10, 11], and more specifically on composite laminates [12–14]. The strength of high-speed DIC

is that it is able to simultaneously measure the response over a wide measurement, providing higher spatial density than individual contacting sensors or laser vibrometers, but, on the other hand, its accurateness is reduced as a consequence of the low displacements, especially at high frequencies, for which the structure's response is too close to, or even below, the noise level of the camera-based measurement system [15, 16].

In the present paper, the development of a numerical model, updated through modal parameters experimentally obtained, is presented. To obtain the modal characteristics of the plates, a modal testing was performed using alternatively: i) a roving hammer exciting the plates at evenly distributed positions, and a mono-axial accelerometer attached to a single degree of freedom (DoF) reference point; ii) two high-speed cameras that simultaneously record the whole surface of the plates during and after the excitation of a hammer, in a single excitation point, for later analysis using DIC. In both cases, vibration data are treated to obtain modal characteristics of the plates by Modal Analysis of Civil Engineering Constructions (MACEC) program [17].

After modal identifications, considerable discrepancies between the numerically calculated and the corresponding experimentally measured modal characteristics of the plates have been identified. Then, global characteristics of the plate for which a certain uncertainty exists were updated. Model updating techniques have been widely applied to adjust theoretical structural models using modal data obtained experimentally during the last three decades, both in civil engineering and more recently for composite plates. Model updating procedure can be treated as a problem of optimization, in

which the weighted differences between experimental and theoretical values of some of the modal characteristics of the structure are computed to obtain the objective function. As a result of the whole process, a physically more accurate model is obtained on which discrepancies with the corresponding experimentally measured modal parameters are drastically reduced. Experimental results obtained from the first experimental method using a roving hammer and accelerometers, together with the consequent model updating, has been already presented in [18]. This paper is then focused on the modal analysis of data coming from DIC and the comparison of the results of the whole process obtained with the alternative experimental techniques. The description of the specimens of carbon/epoxy composite plates used for the work and the test procedures are reported in Section 2. In section 3 the reference numerical models are described. Subsequently, a summary of the results of experimental modal analysis is included in Section 4. Section 5 is dedicated to the description of model updating. Previous results are compared and discussed in section 6. Finally, the conclusions are presented in the last section.

2. Test procedure

The experimental programme involved mainly the experimental modal testing, combining the multiple-input/single-output (MISO) technique, and the single-input/multiple-output (SIMO) process. MISO was performed by using traditional output from accelerometers and a roving hammer, while SIMO was performed using high-speed camera and 3D DIC. These tests were completed with Ultrasonic Inspection (UI) which allowed determining

the real value of thickness of the plates and assessing the absence of damage (delamination) and Quasi Static Loading (QSL) to measure the real stiffness of the laminates. Two sets of composite plates have been studied in the present work: a first driven set of plates with 21 plies, and a second benchmarking set of plates with 32 plies.

2.1. Specimen description

A total of sixteen composite plate specimens composed of AS4 carbon fibres embedded in an 8552 resin epoxy matrix manufactured by HEXCEL have been used. The quasi-isotropic laminated plates were composed of 21 and 32 unidirectional prepeg laminae with a theoretical thickness of 0.19 mm. Driven set has a symmetric stacking sequence (45/-45/90/0/90/-45/45/90/0/90/0)s' while in benchmarking set is (45/-45/90/0/90/-45/45/90/0/90/45/-45/90/90/-45/45)s, resulting in a nominal thickness of the plates of approximately 4 and 6 mm, with a theoretical uniform cross-section over the entire surface. The plates have been cut to obtain 300 x 300 mm2 specimens (Fig. 1). Curing was performed following a standard autoclave procedure by the "Instituto Nacional de Técnicas Aeroespaciales (INTA)". Nominal properties of the laminae provided by the manufacturer are shown on Table 1 (where 1 axis is coincident with the fibre direction).

2.2. Vibration measurements using roving hammer and accelerometers

To obtain the modal characteristics of the plates, a modal testing was performed under free boundary conditions (by suspending the plates vertically with a nylon thread), using a roving hammer exciting the plates at 121 degrees of freedom (DoFs) evenly distributed in both directions (every 25

Table 1: Nominal properties of the plies given by the manufacturer

Property	**Value**
Young modulus in fibre direction ($E_1 1$)	139 GPa
Young modulus in transverse direction ($E_2 2 = E_3 3$)	9 GPa
Shear modulus $G_{12} = G_{13}$	5 GPa
Shear modulus (G_{23})	4.5 GPa
Poisson's ratio ($\nu_{12} = \nu_{13} = \nu_{23}$)	0.3089
Density (ρ)	1580 kg/m^3

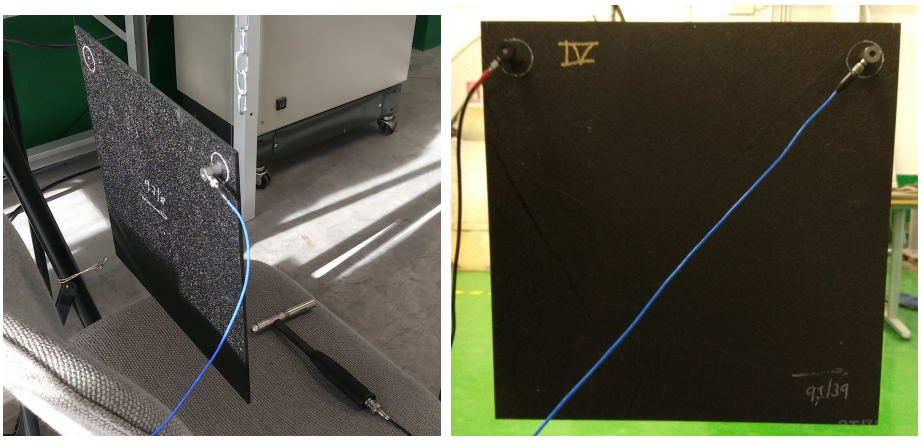

(a) Set-up using 1 accelerometer (b) Set-up using 2 accelerometer

Figure 1: Set-up of vibration measurements using roving hammer and accelerometers

mm). For this study, only dominant vibration responses in the out-of-plane direction were taken into account. Then, mono-axial accelerometers measuring vibration in the out-of-plane direction were used, one (in the case of the driven set) or two (in the case of the benchmarking set) attached to a single DoF reference point [points 1 on the corner of the plate, or points 1 and 11 on both corners of the plates, as seen in Fig. 1].

Three channels of the data acquisition system have been used, one for the

exciter hammer, and the other for the accelerometers. The characteristics of accelerometers and hammer are the following:

- Accelerometers: PCB Piezotronics model 352C33; sensitivity 10.19 and 10.27 mV/m/s2; Measuring range 0.5-10000 Hz
- Hammer:PZB Piezotronics model 086C03; sensitivity 2.25 mV/N; measurement range 2224 N pk; mass 0.16 kg.

Three seconds of the signals after the excitation are recorded at a sampling frequency of 10 kHz. Four plates of the driven set have been tested, with a nominal thickness of 4 mm, and six of the benchmarking set, with a nominal thickness of 6 mm.

2.3. Vibration measurements using 3D DIC

This complementary modal testing was performed on the specimens previously tested, adding another three plates to every set (for a total of seven in the driven set and nine in the benchmarking set). Free boundary conditions were simulated again by suspending the plates vertically as shown in Fig. 2, on which the whole set-up of vibration measurements using 3D DIC is displayed. A single-input excitation was introduced by the same hammer used in previous tests in a corner of the pates. Two high speed cameras Photron FASTCAM SA-Z type 2100K-M-32GB mounted on tripods were used to capture the stereographic images. In order to capture effective images for the DIC algorithm, sticky-backed papers with a random speckle pattern were adhered to the investigated surface of the plates. It can be considered that the additional mass or stiffness of the paper did not change the modal results.

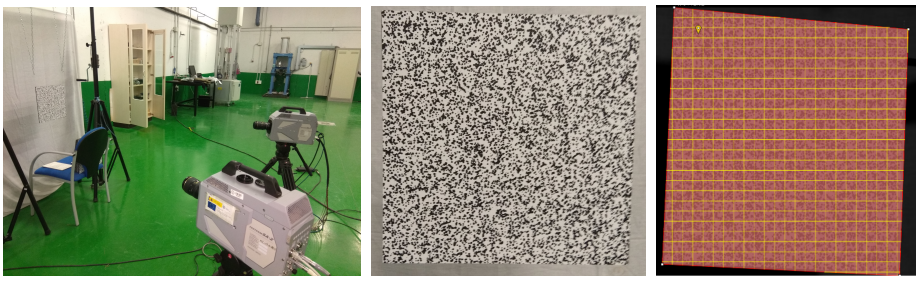

(a) 3D DIC Set-up (b) Speckle pattern (c) Subset size

Figure 2: Set-up of vibration measurements using 3D DIC

The capturing frame rate was initially set to 9000 Hz. However, once it was verified that the experimental method did not allow the identification of modes for frequencies higher that 1500 Hz, it was reduced to 3000 Hz in a second set of tests. The size of individual frames was 768x768 pixels. High intensity illumination for the whole area and exposure times of 1/100000s were used. The hammer is connected to the trigger of the cameras, ensuring that the measurement of the force in the hammer and the recording of the cameras are started automatically simultaneously. Both, the force in the hammer and the images were collected during 100 ms before the excitation and 3 seconds after it. Thus, 27900 pairs of images were collected in the tests performed at 9000Hz of sampling rate, and 9300 in the case of tests performed at 3000Hz.

The speckle pattern for the DIC process was designed according to the resolution of the cameras and the specimen area. Given that the resolution selected was 768x768 px and the area recorded was around 350x350 mm the spatial resolution per pixel was 0.456 mm/px. According to [19, 20] the optimum pattern size is about 3-5 px in order to avoid aliased images and have

low error measurements. In addition, given that the DIC used in this research is stereocorrelation (2 cameras) the Field of View (FOV) of the cameras are not constant, thus the minimum particle size selected was 4 px or 1.82 mm for the spatial resolution during the test. In order to generate a random speckle pattern along the specimen and obtain the maximum contrast between the black dots and the white background, a python code [21] which generates random circular size particles between 4-6 px (1.8 - 2.8 mm) and a random location was coded. The final result is a speckle pattern with circular and conglomerated of circles of random shapes particles, with a minimum size of 4 px. The result was printed using a laser printer onto a paper sticker. Finally, the stickers were applied to all the specimens.

Full-field out-of-plane motion that will be analysed for modal parameter estimation was then obtained by using the Correlated Solutions Vic-3D software. Fig. 3 shows the displacement maps for three different instants of the recorded time. It can be observed that 3D-DIC makes possible to obtain a very precise map of displacements (in this case a range of around $\pm$5mm out-of-plane displacements), which demonstrates the sensitivity of the system.

A quite dense grid of 441 measurements points evenly distributed in both directions every 12.5 mm was established. Fig. 4 shows the grid and an example of the obtained displacements for one of the points. Alternatively, to compare computation time and results, for one of the plates a less dense grid (221 measurements points evenly distributed in both directions every 25 mm, i.e. the same grid used for measurements using roving hammer) and a denser one (1681 measurements points evenly distributed in both directions

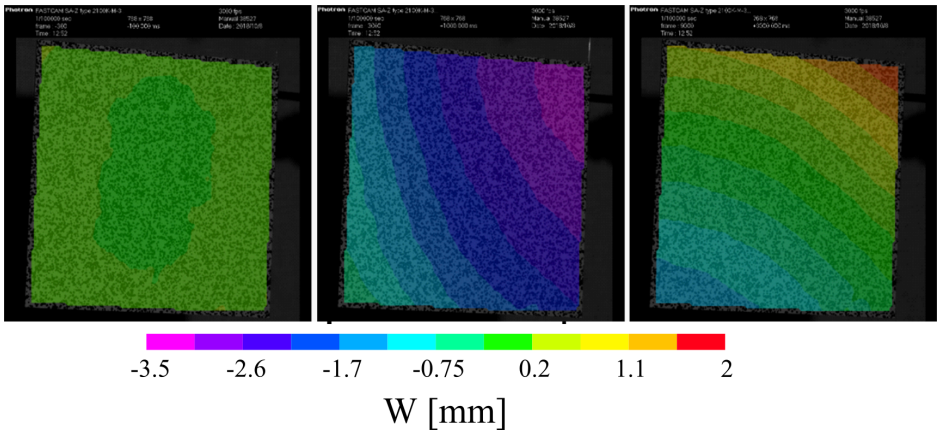

Figure 3: Measured full field out of plane displacement (W) under the excitation of the impulse hammer (before and after excitation 1s and 3 s)

every 6.25 mm, i.e. a grid which corresponds to the FEM mesh) were used. The computation times is not critical considering that varied from 5 min, for the less dense grid, to 12 minutes for the densest one (in a desktop computer).

3. Reference FEM model

The results of the experimental modal estimation will be compared with the results of the modal identification performed through a finite element model of the plates, for which ANSYS software has been used. Given that the goal is to obtain a versatile model that could eventually be used to simulate the presence of intra and interlaminar damage, it is advisable to have at least an element in the thickness of each ply, being possible to model the disconnection between the nodes of the mesh in the interfaces between plies (to model delamination). With this objective, the type of element that best fits the objectives of the model is the hexahedron. For this reason, the SOLID45 element has been used. It is an element with 8 nodes and 3

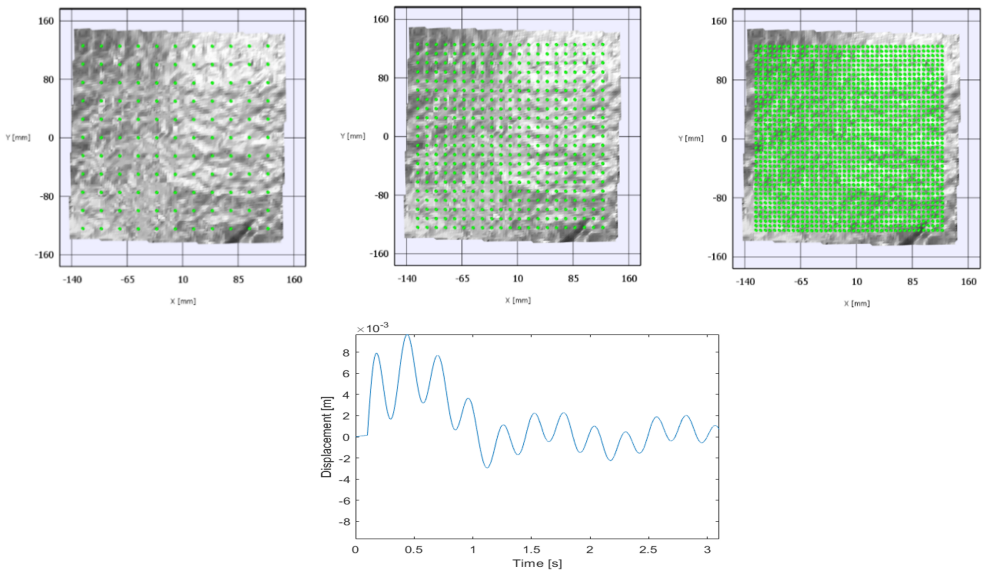

Figure 4: Three used grids of measurement points and example of the obtained displacements for one point

DoF per node. Additionally, mass elements have been included to idealize the presence of the accelerometers used in the experimental determination of the modal characteristics (Fig. 5). This mass, although small (it is 5.8 g.), cannot be considered as negligible and must be included in the model to obtain a greater approximation between theoretical and experimental results, especially for some of the modal forms. The smaller dimension of the element will coincide with the thickness of each of the 21 plies or 32 plies of the plates, that is, 0.19 mm. Regarding the larger dimension, a sensitivity analysis was carried out with values of the element size between 25 and 2.5 mm [18]. After this analysis, it has been established that a size of 6.5 mm is adequate, combining a sufficient precision without increasing the computational cost. The result is the fine mesh that can be seen in Fig. 5.

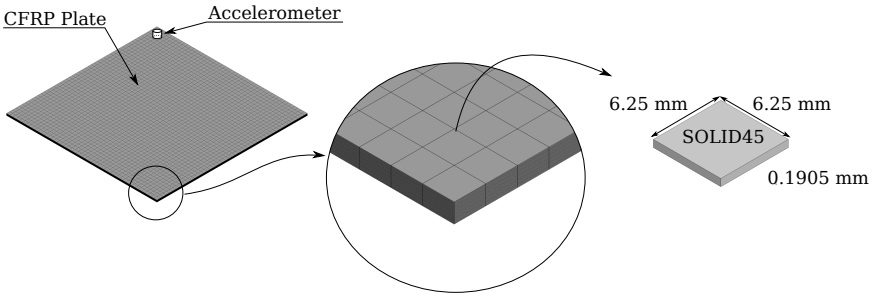

Figure 5: FEM of the plates: position of the mass element that idealizes the accelerometer and mesh

With this model, the first 34 natural frequencies represented in Table 2 are obtained, in which the type (a, b) indicates the number of nodal lines parallel to the crosswise and lengthwise direction of the transverse corresponding mode shapes (as shown in Fig. 6).

4. Modal analysis

The vibration data are treated by MACEC. For modal identification the poly-reference least squares complex frequency domain (pLSCF) algorithm and stochastic subspace identification (SSI) have been used [17].

4.1. Vibration measurements using roving hammer and accelerometers

A parametric modal identification has been carried out using the pLSCF method in MACEC. 22 modes have been identified in the case of the driven set of plates, as shown in Fig. 7, and 19 modes in the case of the benchmarking set, as shown in Fig. 8.

In those tables a comparison with the results obtained from the FEM is included, in terms of differences of natural frequencies and modal assurance

Table 2: 30 first natural frequencies predicted by FEM

Driven set (4mm thickness)				Benchmarking set (6mm thickness)			
N°	**Type**	f_1 **(Hz)**	f_2 **(Hz)**	**N°**	**Type**	f_1 **(Hz)**	f_3 **(Hz)**
1	(1 1)	173.9	170.6	1	(1 1)	249.2	242.7
2	(0 2)	222.3	222.0	2	(0 2)	342.9	342.0
3	(2 0)	306.1	301.7	3	(2 0)	465.0	456.3
4	(1 2)	422.6	417.7	4	(1 2)	615.2	605.1
5	(2 1)	447.0	442.0	5	(2 1)	659.6	649.0
6	(0 3)	677.3	674.0	6	(0 3)	1014.4	1008.3
7	(3 0)	799.9	793.1	7	(2 2)	1160.8	1145.7
8	(2 2)	803.6	801.5	8	(1 3)	1215.4	1212.0
9	(1 3)	822.7	821.0	9	(3 0)	1223.3	1218.7
10	(3 1)	975.2	966.3	10	(3 1)	1449.5	1432.3
11	(2 3)	1287.5	1283.5	11	(2 3)	1856.2	1846.2
12	(0 4)	1314.2	1313.5	12	(3 2)	1945.4	1937.2
13	(3 2)	1336.5	1332.8	13	(0 4)	1959.9	1958.6
14	(1 4)	1498.0	1493.7	14	(1 4)	2198.7	2190.8
15	(4 0)	1569.5	1568.6	15	(4 0)	2374.2	2372.1
16	(4 1)	1699.3	1696.4	16	(4 1)	2542.8	2536.7
17	(3 3)	1904.0	1900.7	17	(3 3)	2732.2	2723.0
18	(2 4)	1941.3	1939.0	18	(2 4)	2799.0	2795.7
19	(4 2)	2127.3	2123.3	19	(4 2)	3099.9	3092.9
20	(0 5)	2185.0	2184.6	20	(0 5)	3223.9	3222.2
21	(1 5)	2317.5	2316.9	21	(1 5)	3399.4	3396.8
22	(5 0)	2560.4	2559.2	22	(3 4)	3712.5	3707.6
23	(3 4)	2631.2	2630.2	23	(4 3)	3862.0	3858.3
24	(4 3)	2696.5	2694.3	24	(5 0)	3874.9	3872.8
25	(5 1)	2711.7	2710.8	25	(5 1)	4023.1	4019.5
26	(2 5)	2818.9	2817.9	26	(2 5)	4049.7	4047.4
27	(5 2)	3097.0	3096.1	27	(5 2)	4515.9	4513.3
28	(0 6)	3245.3	3239.4	28	(0 6)	4739.1	4723.2
29	(1 6)	3400.8	3391.5	29	(4 4)	4909.0	4906.0
30	(4 4)	3458.0	3457.1	30	(1 6)	4938.3	4917.0

Note: f_1: without accelerometer mass; f_2: with one accelerometer; f_3: with two accelerometers

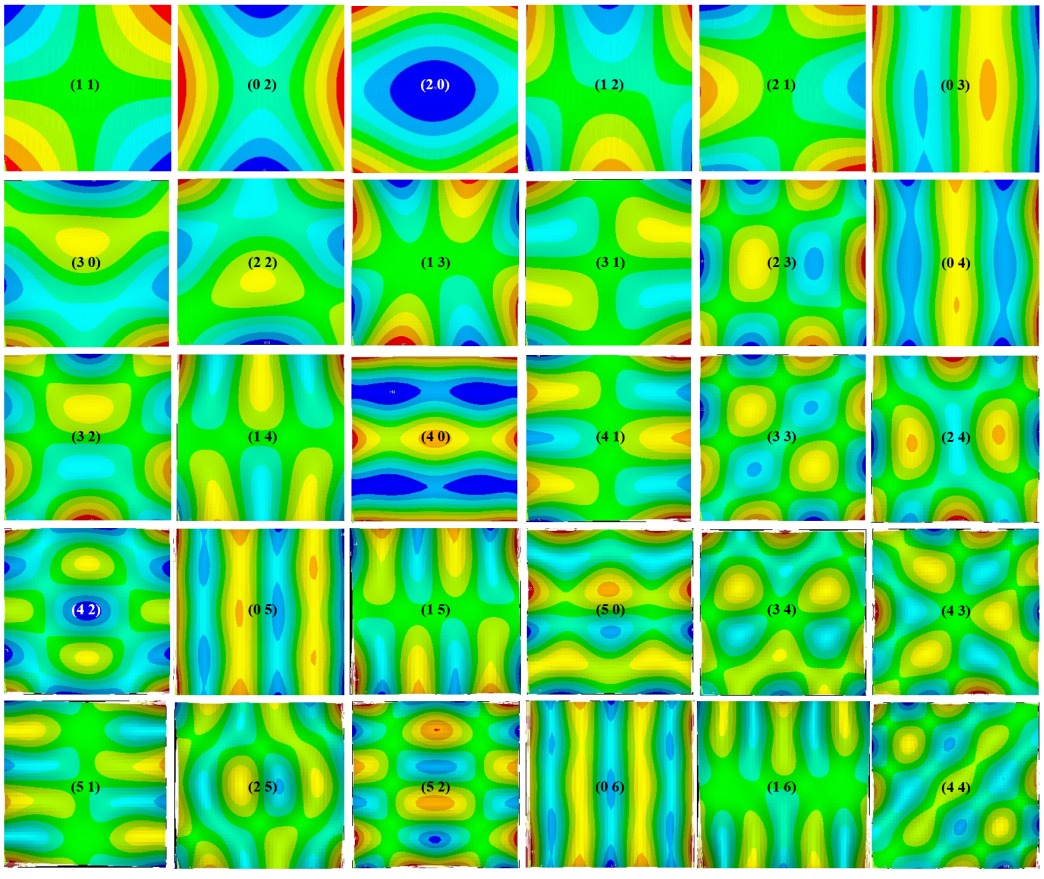

Figure 6: Mode shapes obtained from FEM

	Frequencies Hz)										MAC			
Type	Initial FEM (f_2)			Plate 1	Plate 2	Plate 3	Plate 4	μ	σ	Diff	Plate 1	Plate 2	Plate 3	Plate 4
(1 1)	1	170,6	1	153	155	153	155	154	0,7%	10,8%	0,99	0,97	0,95	0,95
(0 2)	2	222,0	2	206	207	207	207	207	0,2%	7,3%	0,98	0,99	0,99	0,99
(2 0)	3	301,7	3	274	274	275	271	273	0,6%	10,4%	0,98	0,99	0,99	0,81
(1 2)	4	417,7	4	380	382	384	382	382	0,3%	9,4%	0,92	0,94	0,97	0,92
(2 1)	5	442,0	5	401	401	403	401	401	0,2%	10,2%	0,92	0,94	0,85	0,92
(0 3)	6	674,0	6	618	623	624	621	622	0,3%	8,4%	0,97	0,99	0,99	0,99
(3 0)	7	793,1	7	713	716	722	716	717	0,5%	10,7%	0,85	0,79	0,88	0,90
(1 3)	9	821,0	8	751	753	756	753	753	0,2%	9,0%	0,78	0,85	0,87	0,91
(3 1)	10	966,3	9	858	865	870	865	864	0,5%	11,8%	0,83	0,99	0,99	0,99
(2 3)	11	1283,5	10	1174	1174	1177	1173	1174	0,1%	9,3%	0,89	0,96	0,95	0,95
(3 2)	13	1332,8	11	1216	1215	1218	1210	1215	0,2%	9,7%	0,78	0,86	0,79	0,55
(1 4)	14	1493,7	12	1358	1359	1359	1359	1359	0,0%	9,9%	0,90	0,96	0,95	0,99
(4 0)	15	1568,6	13	1444	1442	1423	1425	1433	0,7%	9,4%	0,80	0,93	0,96	0,90
(4 1)	16	1696,4	14	1563	1562	1529	1525	1545	1,2%	9,8%	0,77	0,88	0,92	0,91
(3 3)	17	1900,7	15	1742	1738	1744	1737	1740	0,2%	9,2%	0,85	0,91	0,91	0,96
(2 4)	18	1939,0	16	1780	1777	1783	1768	1777	0,3%	9,1%	0,75	0,19	0,83	0,90
(4 2)	19	2123,3	17	1942	1930	1929	1913	1928	0,5%	10,1%	0,84	0,80	0,92	0,92
(0 5)	20	2184,6	18	1985	1970	2003	1990	1987	0,6%	9,9%	0,12	0,53	0,41	0,40
(1 5)	21	2316,9	19	2084	2084	2093	2108	2092	0,5%	10,7%	0,33	0,61	0,10	0,50
(3 4)	23	2630,2	20	2404	2410	2410	2397	2405	0,2%	9,4%	0,65	0,38	0,51	0,64
(4 3)	24	2694,3	21	2471	2466	2472	2465	2469	0,1%	9,1%	0,63	0,85	0,84	0,88
(0 6)	28	3239,4	22	2955	2982	2974	2982	2973	0,4%	8,9%	0,64	0,80	0,89	0,24
								μ =	0,4%	9,7%	0,78	0,82	0,84	0,82
								max =	1,2%	11,8%				

Figure 7: Natural frequencies obtained from vibration measurements using accelerometers for the driven set (4 mm) of plates

	Frequencies (Hz)											MAC					
Type	Initial FEM (f_3)			Plate 1	Plate 2	Plate 3	Plate 4	Plate 5	Plate 6	μ	σ	Diff	Plate 1	Plate 2	Plate 3	Plate 4	Plate 5	Plate 6
(1 1)	1	242,7	1	224	224	225	226	226	225	225	0,4%	7,8%	0,99	1,00	0,98	1,00	1,00	1,00
(0 2)	2	342,0	2	317	318	322	321	323	322	321	0,6%	6,7%	0,99	0,99	0,99	0,99	1,00	0,99
(2 0)	3	456,3	3	422	423	423	426	427	426	424	0,4%	7,6%	0,99	0,99	0,97	0,99	0,99	0,99
(1 2)	4	605,1	4	558	559	561	564	565	563	562	0,5%	7,7%	0,99	0,99	0,96	0,99	0,98	1,00
(2 1)	5	649,0	5	599	600	599	605	605	604	602	0,4%	7,8%	1,00	1,00	0,95	1,00	0,68	1,00
(0 3)	6	1008,3	6	932	932	938	942	946	944	939	0,6%	7,4%	0,99	0,99	0,97	0,99	0,97	0,99
(2 2)	7	1145,7	7	1059	1059	1063	1067	1069	1068	1064	0,4%	7,7%	0,99	0,99	0,93	0,99	0,96	0,99
(1 3)	8	1212,0	8	1127	1133	1123	1140	1136	1138	1133	0,5%	7,0%	0,92	0,92	0,70	0,75	0,88	0,80
(3 1)	10	1432,3	9	1326	1331	1313	1338	1318	1337	1327	0,7%	7,9%	0,99	0,99	0,92	0,99	0,91	0,99
(2 3)	11	1846,2	10	1718	1710	1720	1731	1715	1720	1719	0,4%	7,4%	0,98	0,98	0,95	0,98	0,86	0,97
(3 2)	12	1937,2	11	1799	1798	1785	1814	1815	1812	1804	0,6%	7,4%	0,94	0,89	0,90	0,92	0,83	0,94
(1 4)	14	2190,8	12	2046	2034	2056	2064	2010	2063	2045	0,9%	7,1%	0,96	0,96	0,91	0,95	0,89	0,93
(4 0)	15	2372,1	13	2209	2209	2227	2223	2242	2230	2223	0,5%	6,7%	0,88	0,94	0,72	0,90	0,70	0,89
(4 1)	16	2536,7	14	2363	2362	2364	2379	2407	2384	2376	0,7%	6,7%	0,95	0,96	0,54	0,92	0,18	0,87
(3 3)	17	2723,0	15	2529	2526	2528	2546	2549	2533	2535	0,4%	7,4%	0,95	0,92	0,90	0,92	0,13	0,89
(2 4)	18	2795,7	16	2594	2600	2606	2621	2629	2611	2610	0,5%	7,1%	0,90	0,91	0,91	0,89	0,11	0,80
(4 2)	19	3092,9	17	2875	2874	2884	2893	2898	2886	2885	0,3%	7,2%	0,85	0,83	0,80	0,82	0,35	0,61
(3 4)	22	3707,6	18	3441	3437	3442	3471	3462	3449	3450	0,4%	7,5%	0,74	0,73	0,63	0,73	0,29	0,60
(4 3)	23	3858,3	19	3580	3579	3585	3617	3612	3601	3596	0,4%	7,3%	0,64	0,62	0,69	0,71	0,47	0,35
										μ =	0,5%	7,2%	0,93	0,93	0,86	0,92	0,69	0,87
										max =	0,9%	7,5%						

Figure 8: Natural frequencies obtained from vibration measurements using accelerometers for the benchmarking set (6 mm) of plates

criterion (MAC) values, that provide a scalar correlation criterion that indicates the degree of coherence or correlation between two modal vectors [22]. To obtain those MAC values a mode pairing has been necessary. Mode pairing is the process by which the vibration modes of the numerical model that correspond to the modes extracted from the experimental analysis are identified. This pairing is not immediate because the numbers of the numerical and experimental modes will not coincide in general. The most commonly used parameter to perform this task is MAC. Thus, for each experimental mode i the corresponding numerical mode J will be the one with the highest MAC value when compared to it; that is, $MAC_{iJ} = max(MAC_{ij})$.

It is generally assumed that values greater than 0.8 indicate an adequate coherence value between experimental and theoretical mode. In Fig. 7 and 8 the MAC values can be seen on the right columns and, as can be observed, the identification is, in general, very clear, since most of the MAC values are higher than 0.8.

On the other hand, it is also important to point out that the differences between the specimens in terms of natural frequencies are very low. That makes possible to process the data of the different specimens as corresponding to different setups of the same test, identifying average values of frequencies and modal forms, which improves the accuracy of the test. This procedure has been done with the four plates of the driven set, obtaining the results shown in Fig. 9. However, for the benchmarking set, even though all the modes have been identified in the six plates again with very stable values of the frequency, it can be pointed out that in the case of three of the plates (1, 2 and 4) MAC values are higher than in the case of plates 3, 5 and 6.

	Test		Initial FEM (f_2)		
Type	Nº	Freq (Hz)	Freq (Hz)	Diff (%)	MAC
(1 1)	1	154	170.58	10.8%	0.99
(0 2)	2	207	221.97	7.3%	1.00
(2 0)	3	273	301.68	10.4%	0.99
(1 2)	4	382	417.72	9.4%	0.95
(2 1)	5	401	442.04	10.2%	0.93
(0 3)	6	622	673.97	8.4%	0.99
(3 0)	7	717	793.13	10.7%	0.91
(1 3)	8	753	821.04	9.0%	0.89
(3 1)	9	864	966.30	11.8%	0.98
(2 3)	10	1174	1283.45	9.3%	0.96
(3 2)	11	1215	1332.77	9.7%	0.84
(1 4)	12	1359	1493.73	9.9%	0.97
(4 0)	13	1433	1568.58	9.4%	0.96
(4 1)	14	1545	1696.37	9.8%	0.96
(3 3)	15	1740	1900.71	9.2%	0.94
(2 4)	16	1777	1939.01	9.1%	0.90
(4 2)	17	1928	2123.27	10.1%	0.93
(0 5)	18	1987	2184.58	9.9%	0.46
(1 5)	19	2092	2316.87	10.7%	0.55
(3 4)	20	2405	2630.17	9.4%	0.74
(4 3)	21	2469	2694.26	9.1%	0.94
(0 6)	22	2973	3239.44	8.9%	0.85
				μ =	**9.7%** **0.89**
				max =	**11.8%**

	Test		Initial FEM (f_3)		
Type	Nº	Freq (Hz)	Freq (Hz)	Diff (%)	MAC
(1 1)	1	225	242.7	8.0%	1.00
(0 2)	2	319	342.0	7.2%	0.99
(2 0)	3	423	456.3	7.8%	1.00
(1 2)	4	561	605.1	7.9%	0.99
(2 1)	5	602	649.0	7.9%	1.00
(0 3)	6	936	1008.3	7.8%	0.99
(2 2)	7	1062	1145.7	7.9%	0.99
(3 0)	8	1134	1218.7	7.5%	0.65
(3 1)	9	1332	1432.3	7.5%	1.00
(2 3)	10	1720	1846.2	7.4%	0.99
(3 2)	11	1804	1937.2	7.4%	0.94
(1 4)	12	2048	2190.8	7.0%	0.98
(4 0)	13	2214	2372.1	7.2%	0.94
(4 1)	14	2368	2536.7	7.1%	0.97
(3 3)	15	2534	2723.0	7.5%	0.97
(2 4)	16	2605	2795.7	7.3%	0.95
(4 2)	17	2881	3092.9	7.4%	0.91
(3 4)	18	3450	3707.6	7.5%	0.86
(4 3)	19	3592	3858.3	7.4%	0.80
				μ =	**7.5%** **0.94**
				max =	**8.0%**

Figure 9: Final natural frequencies obtained from vibration measurements using accelerometers: left) driven set of plates (4 mm); right) benchmarking set of plates (6 mm)

For this reason the data have been processed as corresponding to different setups of the same test, but only using those results corresponding to plates 1, 2 and 4 in the case of the benchmarking set. Fig. 9 shows the results.

Regarding experimental uncertainty in modal identification, it is well known that modal characteristics that are estimated from vibration measurements are subject to variance errors and bias [23]. In this case, in which several specimens have been tested, differences between them provide a first indication of results dispersion. In this sense, as abovementioned, the differences in terms of natural frequencies between specimens are low, with values

of standard deviation of around 0.4% to 0.5%, with a maximum of 1.2% (as can be seen in figure 7 and figure 8). It must be pointed out that at least part of those differences will be due to actual mechanical differences between the specimens and not due to experimental method. Apart from that, however, the experimental process itself can lead to estimate spurious or biased modes and to variance errors in the identification. The comparison with the modal analysis performed on the FEM is useful to avoid spurious mode. Additionally, the stabilization diagrams used by Macec software, which are constructed by choosing a wide range of model orders n for the identification and by plotting all identified modes in a frequency vs. model order diagram is a good way to remove part of the bias error [23]. On the other hand, variance errors cannot be removed but only estimated. Stabilisation diagrams in Macec can be plotted considering a set of different stabilisation criteria. One of this stabilisation criteria is the variance error in frequency. In the stabilisation diagrams considering default values for all stabilisation criteria that, in the case of the variance error in frequency, is 1%, identified modes appear in clear columns of stable modes. Nevertheless, if stabilisation criterium for variance error in frequency is highly reduced to 0.01%, which means a standard deviation of 0.1% lower than the one existing between specimens, selected modes still appear as stable. This indicates that actual variance errors for estimated modes are very low.

4.2. Vibration measurements using 3D DIC

A parametric modal identification has been carried out in MACEC, using in this case the SSI method. Before this analysis, to assess the practical capacity of the system, considering the sensitivity of the cameras to measure

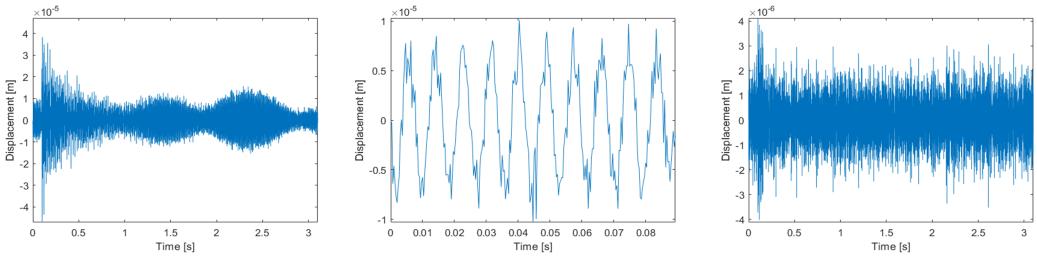

Figure 10: Out-of-plane displacement history obtained by DIC: left) complete time history; center) first 100 ms of measurement before excitation; right) complete time history after low-pass filter

the out-of-plane displacements, displacement history of one point of one of the plates was studied. The displacement time histories are previously processed in two steps: i) to remove the offset of the signals; ii) to remove the low-frequency rigid-body motion using a high-pass filter. After this process the time history shown in Fig. 4 is transformed in the one shown in Fig. 10 left. As can be seen the maximum displacement recorded is of about $40\mu m$. In Fig. 10 center an enlarged figure of the first 100 ms of measurement (before the excitation of the hammer is applied) is shown. Since no external load was applied on the plate, the out-of-plane displacements should be zero, and the measured displacements, up to $10\mu m$, thus can be considered as noise. What it is interesting to see is that if a low-pass filter with a cut-up frequency of 1000 Hz is applied (Fig. 10 right), the displacement amplitude (4 μm) is below this noise floor. Thus, noise will affect mainly higher frequencies.

Fig. 11 compares the FFT spectra of both, acceleration recorded by accelerometers tests and out-of-plane displacements recorded by DIC tests. As can be seen, for low frequencies (clearly under 500 Hz) similar peaks representing natural frequencies of the plates can be identified on both spectra.

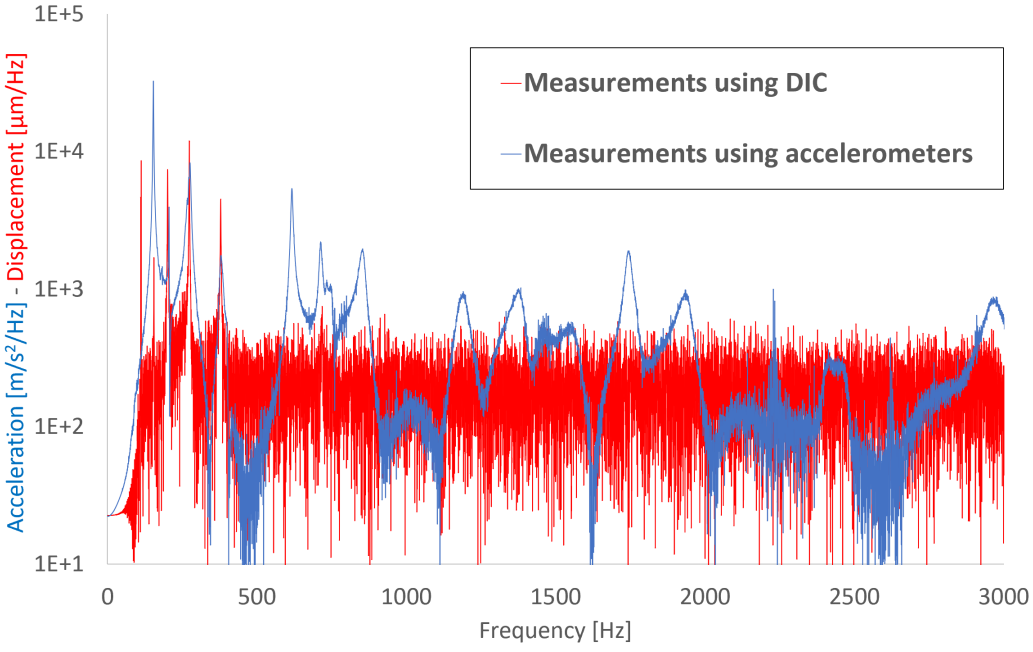

Figure 11: FT spectra of accelerations

However, for higher frequencies, in the case of the results obtained from accelerometer, the analysis will allow to estimate corresponding natural frequencies (as seen in the previous section), but for the spectrum corresponding to the displacements obtained by DIC, the noise level will make almost impossible this estimation. The same phenomenon can be observed in Fig. 12, in which the stabilization diagram obtained from the two measurement methods are compared. Stabilized modes have been picked up (red circles), and they appear grouped in a clearly vertical lines in the diagram usually also corresponding to the peaks of the PSD. However, as can be seen, up to 20 columns of stabilized modes appears in the case of accelerometers measurements, but only 7 in the case of DIC tests.

Fig. 13 and Fig. 14 show the results obtained for the driven and bench-

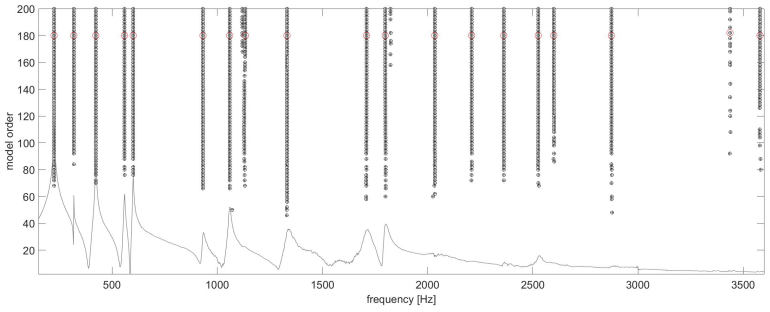

(a) accelerometer measurements using pLSCF

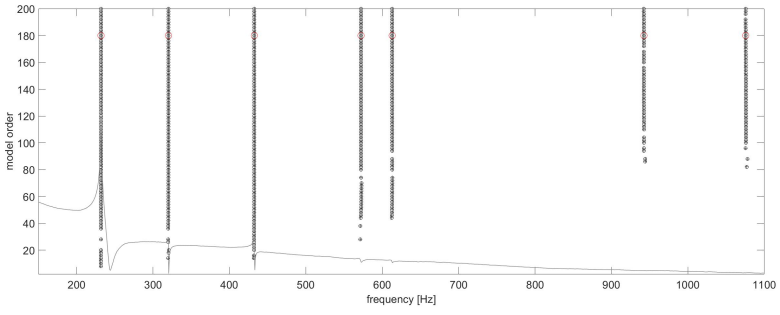

(b) 3D DIC measurements using SSI

Figure 12: Stabilization diagrams

				Frequencies Hz)										MAC						
Type	Initial FEM (f_1)			Plate 1	Plate 2	Plate 3	Plate 4	Plate 5	Plate 6	Plate 7	μ	σ	Diff	Plate 1	Plate 2	Plate 3	Plate 4	Plate 5	Plate 6	Plate 7
(1 1)	1	173,9	1	160	160	161	160	160	160	160	160	0,2%	8,5%	0,99	0,99	0,96	0,98	1,00	1,00	1,00
(0 2)	2	222,3	2	208	208	207	208	208	207	208	208	0,2%	7,0%	0,99	0,99	0,52	0,96	0,98	0,98	0,98
(2 0)	3	306,1	3	282	282	283	281	282	282	283	282	0,2%	8,5%	0,98	0,98	0,85	0,97	1,00	1,00	1,00
(1 2)	4	422,6	4	389	389		389	389	390	391	390	0,2%	8,4%	0,93	0,93		0,95	0,95	0,98	0,98
(2 1)	5	447,0	5	408	410			410	412	415	411	0,5%	8,7%	0,93	0,92			0,96	0,99	0,99
(0 3)	6	677,3	6	631	631	628	628	628	626	629	629	0,3%	7,7%	0,99	0,99	0,81	0,96	0,97	0,97	0,97
(3 0)	7	799,9	7	734	733						734	0,0%	9,0%	0,76	0,73					
(2 2)	8	803,6	8	739	739			737	736		738	0,2%	8,9%	0,80	0,84			0,65	0,96	
(1 3)	9	822,7	9	763	763						763	0,0%	7,8%	0,79	0,86					
(3 1)	10	975,3	10	892	892		890		894	900	894	0,4%	9,1%	0,94	0,94		0,56		0,95	0,95
(2 3)	11	1287,6	11	1187	1187						1187	0,0%	8,4%	0,84	0,85					
(3 2)	13	1336,5	12		1221				1225	1236	1228	0,5%	8,9%		0,50				0,90	0,90
											μ =	0,2%	8,4%	0,90	0,88	0,79	0,90	0,93	0,97	0,97
											max =	0,5%	9,1%							

Figure 13: Natural frequencies obtained from vibration measurements using 3D DIC for the driven set of plates (4 mm thickness)

	Frequencies Hz)													MAC								
Type	Initial FEM (f_1)		Plate 1	Plate 2	Plate 3	Plate 4	Plate 5	Plate 6	Plate 7	Plate 8	Plate 9	μ	σ	Diff	Plate 1	Plate 2	Plate 3	Plate 4	Plate 5	Plate 6	Plate 7	Plate 8	Plate 9
(1 1)	1	249,2	231	232	233	232	234	232	231	231	232	232	0,3%	7,4%	1,00	1,00	1,00	0,99	1,00	1,00	0,99	1,00	1,00
(0 2)	2	342,9	319	320	325	320	325	323	320	320	321	321	0,6%	6,7%	0,98	0,98	1,00	0,98	0,98	0,98	0,98	0,99	0,98
(2 0)	3	465,0	432	433	433	433	437	435	432	433	434	433	0,4%	7,3%	1,00	1,00	0,99	1,00	0,99	1,00	1,00	1,00	1,00
(1 2)	4	615,2	570	572	574	571	578	575	573	571	575	573	0,4%	7,3%	0,97	0,98	0,99	0,96	0,96	0,97	0,98	0,98	0,98
(2 1)	5	659,6	612	613	613	614	619	620	612	613	614	615	0,5%	7,3%	0,98	0,99	0,99	0,98	0,97	0,58	0,99	0,99	0,99
(0 3)	6	1014,4	940	942	953	943	957	954	944	943	950	947	0,6%	7,1%	0,90	0,95	0,98	0,88	0,87	0,94	0,93	0,95	0,92
(2 2)	7	1160,8	1093	1070	1080	1083						1081	0,8%	7,3%	0,18	0,87	0,94	0,21					
												μ =	0,5%	7,2%	0,86	0,97	0,98	0,86	0,96	0,91	0,98	0,98	0,98
												max =	0,8%	7,4%									

Figure 14: Natural frequencies obtained from vibration measurements using 3D DIC for the benchmarking set of plates (6 mm thickness)

marking sets respectively. As can be seen and previously anticipated, the number of identified modes is drastically reduced, up to 12 modes in the cases of the driven set (with plates in which only four modes have been identified) and only 7 in the case of the benchmarking set.

It can be observed that once again the differences between the specimens in terms of natural frequencies are very low. On the other hand, in those tables, mode pairing with the modes of the numerical model is included, and once more with most of the MAC values higher than 0.8, but encountering in some identified modes quite reduced values. Thus, to obtain an experimental baseline, averaged values of the frequencies obtained from all the plates have been considered, but in terms of mode shapes, retained values come from the plates in which higher MAC values have been encountered. Fig. 15 shows the final results.

Fig. 16 shows the comparison between the mode shapes obtained from the FEM model and those identified experimentally (also including those obtaining using roving hammer and accelerometers). It can be observed that the shapes obtained from 3D DIC not only have a higher definition, because it is possible to obtain modal displacement in a much denser grid of points, but are also smoother, at least in the case of the modes of lower frequencies.

	Test		Initial FEM (f_1)		
Type	Nº	Freq (Hz)	Freq (Hz)	Diff (%)	MAC
(1 1)	1	160	173.9	8.5%	1.00
(0 2)	2	208	222.3	7.0%	0.99
(2 0)	3	282	306.1	8.5%	1.00
(1 2)	4	390	422.6	8.4%	0.98
(2 1)	5	411	447.0	8.7%	0.99
(0 3)	6	629	677.3	7.7%	0.99
(3 0)	7	734	799.9	9.0%	0.76
(2 2)	8	738	803.6	8.9%	0.96
(1 3)	9	763	822.7	7.8%	0.86
(3 1)	10	894	975.3	9.1%	0.95
(2 3)	11	1187	1287.6	8.4%	0.85
(3 2)	12	1228	1336.5	8.9%	0.90
			μ =	**8.4%**	**0.93**
			max =	**9.1%**	

	Test		Initial FEM (f_1)		
Type	Nº	Freq (Hz)	Freq (Hz)	Diff (%)	MAC
(1 1)	1	232	249.2	7.4%	1.00
(0 2)	2	321	342.9	6.7%	0.99
(2 0)	3	433	465.0	7.3%	1.00
(1 2)	4	573	615.2	7.3%	0.98
(2 1)	5	615	659.6	7.3%	0.99
(0 3)	6	947	1014.4	7.1%	0.95
(2 2)	7	1081	1160.8	7.3%	0.87
			μ =	**7.2%**	**0.97**
			max =	**7.4%**	

Figure 15: Final natural frequencies obtained from vibration measurements using 3D DIC: left) driven set of plates (4 mm); right) benchmarking set of plates (6 mm)

On the other hand, Fig. 17 shows the comparison between experimental mode shapes from measurements with 3D DIC using the three different grids. The differences in computation time for the modal analysis are more important: 2 minutes for the 121 points grid, 5 minutes for the 441 points one and 35 minutes for the densest grid.

In order to compute the accuracy differences for the mode shapes obtaining with every grid, compared to the FEM ones, a surface fitting was performed, as shown in Fig. 18 and 19. This allows to compute the square error between different mode shapes homogeneously, independently of the number of points of the grids. The results of this computation for the first three modes is shown in Fig. 3. As can be seen, there is a significant difference between the modes obtained using roving hammer and accelerometer and those from DIC. However, the density of the grid seems not to have a great influence.

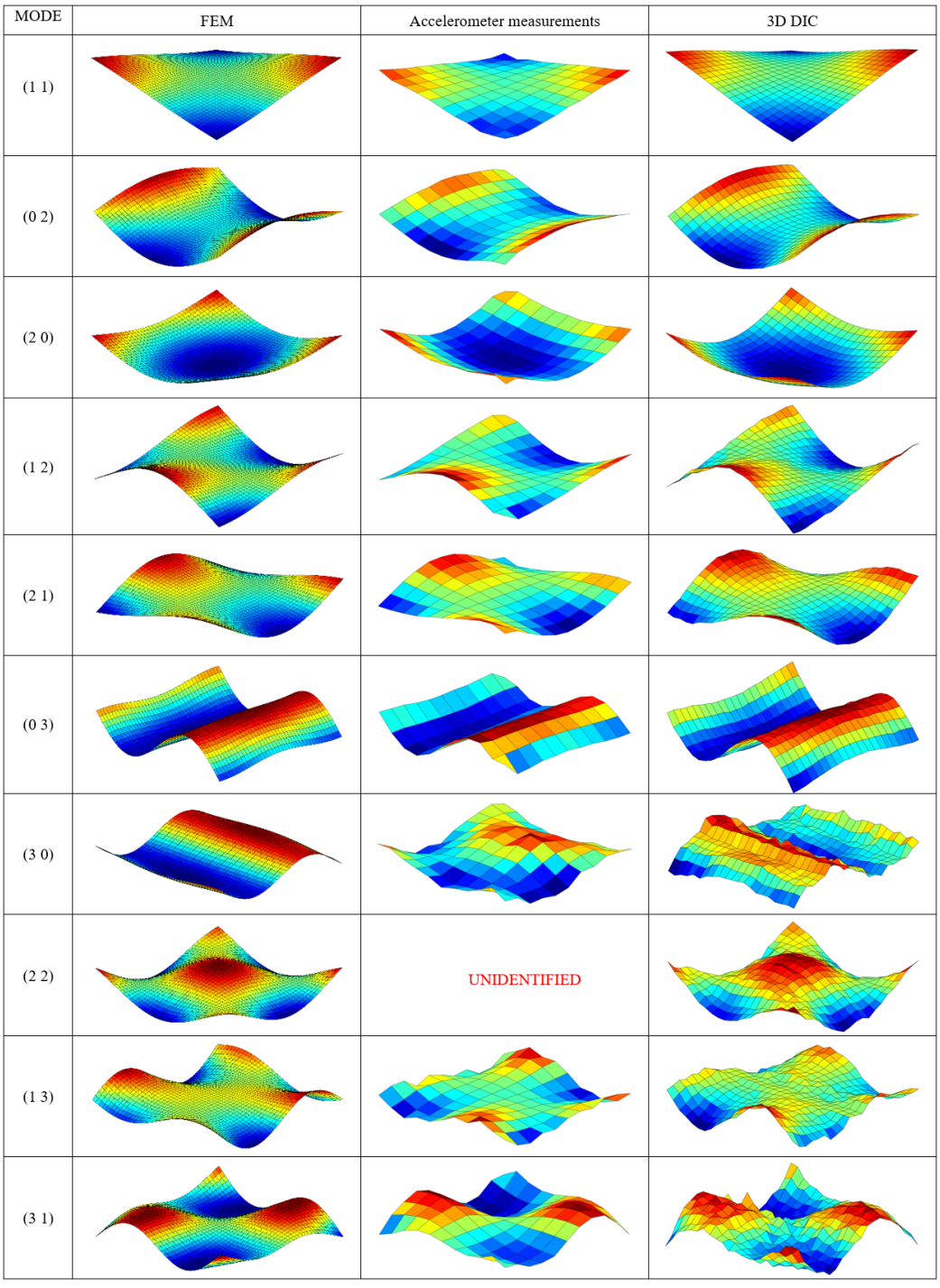

Figure 16: First 10 numerical and experimental mode shapes of driven set of plates

Mode	121 points grid	441 points grid	1681 points grid
(1 1)	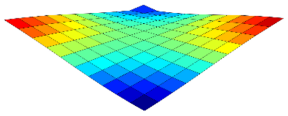	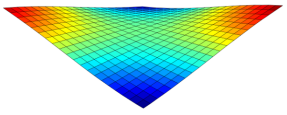	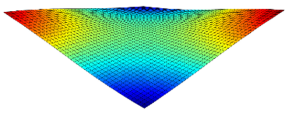
(0 2)	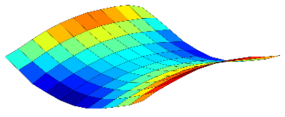	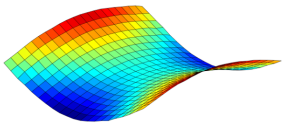	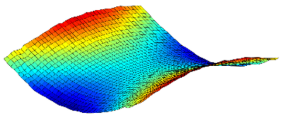
(2 0)	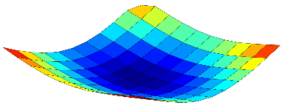	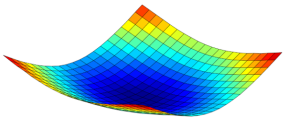	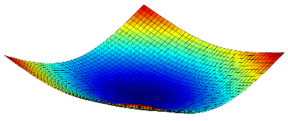

Figure 17: Comparison between experimental mode shapes from measurements with 3D DIC using different grids

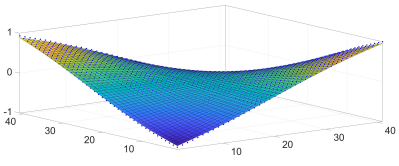

(a) 1681-points grid (DIC)

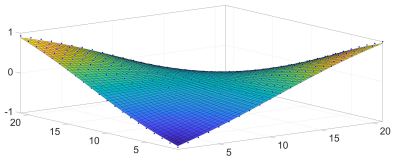

(b) 441-points grid (DIC)

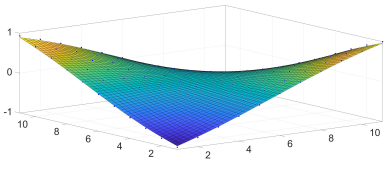

(c) 121-points grid (DIC)

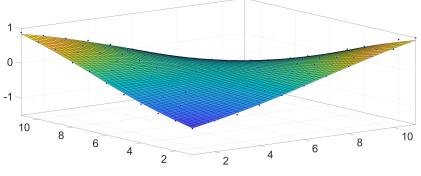

(d) 121-points grid (accelerometers)

Figure 18: Examples of surface fitting of mode 1 shape

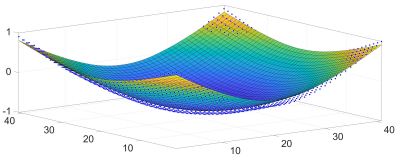

(a) 1681-points grid (DIC)

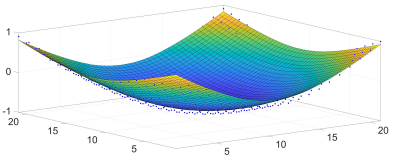

(b) 441-points grid (DIC)

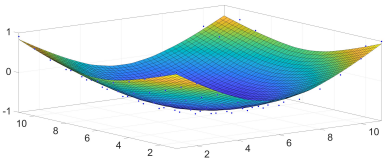

(c) 121-points grid (DIC)

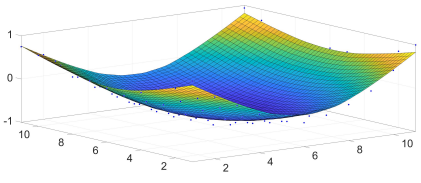

(d) 121-points grid (accelerometers)

Figure 19: Examples of surface fitting of mode 3 shape

Table 3: Square error between experimental mode shape and FEM for different grids and methods

	Square error in Mode shape			
	Mode 1	**Mode 2**	**Mode 3**	**Total**
1681-points grid (DIC)	1.8	16.1	19.8	37.7
441-points grid (DIC)	1.8	16.0	20.7	38.5
121-points grid (DIC)	2.2	14.0	23.2	39.4
121-points grid (Accelerometers)	5.1	28.3	23.7	57.2

Nonetheless, it must be considered that the techniques that are evaluated in the present work are intended to be used for damage identification and localization in the future. In this sense, the investigation of variations in mode shape curvatures has been applied successfully in previous works [24–26]. To be able to use these techniques, it will be relevant the accuracy reached in the values of curvature of the experimental mode shapes. Table 4 shows the results of the computation of the square error between curvature values of experimental mode shape and FEM for different grids and methods. As can be seen, in this case there are very important differences between the degree of accuracy obtained with the different grids. This can be seen graphically in Fig. 20, which shows the comparison between FEM and experimental mode shape curvatures using different grids and techniques. It can be observed how the different grids and methodologies can capture the overall shape of the modes. Nevertheless, the denser the grid of points is, the more accurate the results obtained will be.

Table 4: Square error between curvature values of experimental mode shape and FEM for different grids and methods

	Square error in Mode shape			
	Mode 1	**Mode 2**	**Mode 3**	**Total**
1681-points grid (DIC)	193.6	52.4	21.9	267.9
441-points grid (DIC)	769.2	456.7	4977.0	6202.9
121-points grid (DIC)	2674.0	605.2	4600.0	7879.2
121-points grid (Accelerometers)	954.0	385.2	3134.0	4473.2

Regarding experimental uncertainty using 3D DIC method, again the differences in terms of natural frequencies between specimens are low, with values of standard deviation of around 0.2% to 0.5%, with a maximum of

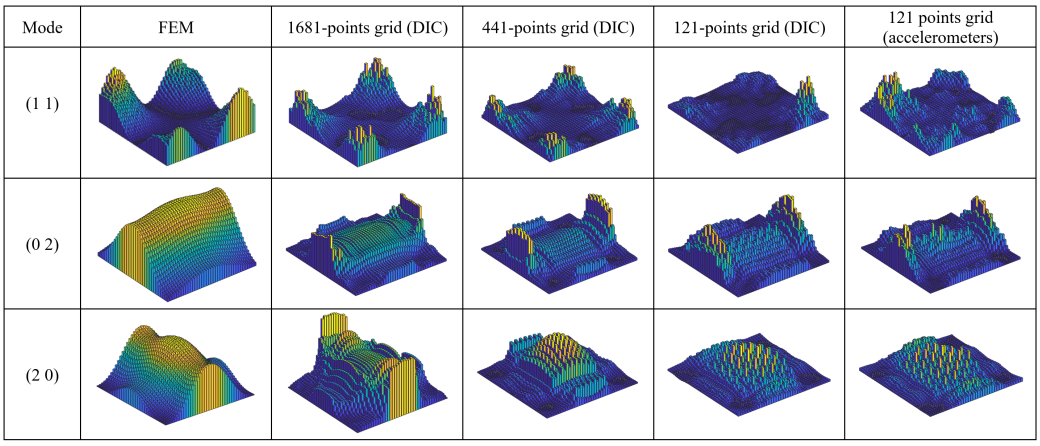

Figure 20: Comparison between FEM and experimental mode shape curvatures using different grids and techniques

0.8% (as can be seen in figure 13 and figure 14). In this case, however, especially for the driven set of plates, for some plates several modes are not identified.

With this method variance errors for estimated modes are very low again. Stabilisation diagrams considering a value of 0.01% for the stabilisation criterium for variance error in frequency, selected modes appear as stable even for this very reduced value of the criterium.

5. Model Updating

Model updating is the process by which some parameters of the numerical models (such as density, thickness of the plies and elastic properties of the composite material) are corrected, based on experimental data (the identified experimental modal parameters in this case), to minimize the deviations of the models from real structural behaviour. The process is usually divided into three main parts: (i) contrast with experimental results, (ii) sensitivity

analysis and (iii) parameter adjustment. This contrast has been presented together with experimental results in the previous section, consisting essentially in the abovementioned process of mode pairing. After mode pairing, a sensitivity analysis is usually performed to determine which parameters of the model have the greatest influence on the responses of interest, in this case the vibration mode shapes and eigenfrequencies. Thus, in the next step, the model updating, only the numerical values of those parameters that are identified to be influential will be adjusted until the objective function is minimized. The sensitivity analysis performed in this work is explained in detail in [18]. It was demonstrated that the three parameters to which the model is more sensitive, are those presented in Table 5. In the updating process they will be subjected to a series of restrictions represented by their upper and lower margins of variation also shown in the table.

Table 5: Parameters to be adjusted

Parameter	**Mean value**	**Limits**	**Units**
Young Modulus Fiber direction (E_1)	139	69.5/208.5	GPa
Density (ρ)	1580	790/2370	Kg/m^3
Lamina thickness	0.191	0.095/0.286	mm

Model updating process will be basically to minimize a function, the so-called "objective function", which evaluates the difference between the experimental results and those obtained from the model. Thus, a zero value of the objective function means that both set of results are coincident. Several methods can be applied to solve this problem. Computational intelligence techniques as neural networks, particle swarm and genetic-algorithm-based methods, simulated annealing or response surface method [27, 28]. Zero-

order methods, as Subproblem approximation method, or gradient-based as the first-order optimization methods, both of them implemented in ANSYS [29], would be an alternative. Both types of strategies have been used in previous works of the authors [30, 31], obtaining similar results. In the present work ANSYS optimization algorithms has been chosen. Although there are various possibilities for defining the objective function, a weighted sum of differences between the experimental modal data (eigen-frequencies and mode shapes) and the corresponding predictions from the model is one of the most common in these kinds of work [31, 32]:

$$f = \sum_{i}^{n} \left[c_i \left| \frac{f_{i,exp} - f_{i,FEM}}{f_{i,exp}} \right| + d_i \left(1 - MAC_i\right) \right] \tag{1}$$

Where:

- n is the number of modes used in the adjustment
- $f_{i,exp}$ and $f_{i,FEM}$ are, respectively, the frequency of the i-th mode identified in the tests and calculated with the numerical model and paired with the previous one through the MAC value
- c_i and d_i are the weighting factors that are used to give more importance to the frequencies characterized with greater precision, if that is the case, and to the criterion depending on the modal forms
- MAC_i is the highest value of the MAC obtained for the i-th mode identified in the tests when compared with the n numerical modes; that is, $MAC_i = max(MAC_{ij})$.

As it was seen in [18], the MAC values are not sensitive to the parameters of the model, thus it is not necessary to include them in the calculation of the objective function, so that all the coefficients d_i will be null. On the other hand, the MAC value can be considered as an indicator of the precision with which the experimental modes have been identified. That is, it is considered a priori that the modes with the lowest MAC have been identified with less precision than those with the high MAC. For this reason, it has been considered appropriate to use the MAC value as a factor for weighting the frequencies. Therefore, the final expression of the objective function will be:

$$f = \sum_{i}^{n} \left[c_i \left| \frac{f_{i,exp} - f_{i,FEM}}{f_{i,exp}} \right| \right] \tag{2}$$

5.1. Model updating using results from accelerometers measurements

As seen in section 4.1, the experimentally identified modes, twenty-two in the case of the driven set (4 mm) and nineteen for the benchmarking set (6 mm), have relatively high values of the MAC, comparing modes shape with those numerically obtained from the theoretical FEM model. However, considerable discrepancies between the corresponding natural frequencies have been encountered, as shown in Fig. 9. After the model updating process presented in [18], the updated values shown in Table 6 were obtained.

Table 6: Adjusted values of the parameters through model updating using results from accelerometers measurements

		Driven Set		Benchmarking set	
Parameter	**Initial value**	**Adjusted value**	**Δ**	**Adjusted value**	**Δ**
E1(GPa)	139	135	-3%	143	3%
Density(Kg/m3)	1580	1623	3%	1644	4%
Lamina thickness (mm)	0.190	0.177	-7%	0.178	-6%

	Test		Initial FEM (f_2)			Updated FEM (f_2)		
Type	Nº	Freq (Hz)	Freq (Hz)	Diff (%)	MAC	Freq (Hz)	Diff (%)	MAC
(1 1)	1	154	170.6	10.8%	0.99	155.4	0.9%	0.99
(0 2)	2	207	222.0	7.3%	1.00	202.4	-2.2%	1.00
(2 0)	3	273	301.7	10.4%	0.99	274.6	0.5%	0.99
(1 2)	4	382	417.7	9.4%	0.95	380.9	-0.3%	0.95
(2 1)	5	401	442.0	10.2%	0.93	403.0	0.5%	0.93
(0 3)	6	622	674.0	8.4%	0.99	614.6	-1.1%	0.99
(3 0)	7	717	793.1	10.7%	0.91	723.1	0.9%	0.90
(1 3)	8	753	821.0	9.0%	0.89	749.4	-0.5%	0.89
(3 1)	9	864	966.3	11.8%	0.98	881.2	1.9%	0.98
(2 3)	10	1174	1283.5	9.3%	0.96	1172.0	-0.2%	0.96
(3 2)	11	1215	1332.8	9.7%	0.84	1216.9	0.2%	0.84
(1 4)	12	1359	1493.7	9.9%	0.97	1364.0	0.4%	0.98
(4 0)	13	1433	1568.6	9.4%	0.96	1431.4	-0.1%	0.96
(4 1)	14	1545	1696.4	9.8%	0.96	1548.8	0.3%	0.96
(3 3)	15	1740	1900.7	9.2%	0.94	1736.9	-0.2%	0.94
(2 4)	16	1777	1939.0	9.1%	0.90	1772.1	-0.3%	0.90
(4 2)	17	1928	2123.3	10.1%	0.93	1940.1	0.6%	0.93
(0 5)	18	1987	2184.6	9.9%	0.46	1996.2	0.5%	0.46
(1 5)	19	2092	2316.9	10.7%	0.55	2118.1	1.2%	0.55
(3 4)	20	2405	2630.2	9.4%	0.74	2405.1	0.0%	0.74
(4 3)	21	2469	2694.3	9.1%	0.94	2464.4	-0.2%	0.94
(0 6)	22	2973	3239.4	8.9%	0.85	2963.7	-0.3%	0.85
			μ =	**9.7%**	**0.89**		**0.6%**	**0.89**
			max =	**11.8%**			**2.2%**	

	Test		Initial FEM (f_3)			Updated FEM (f_3)		
Type	Nº	Freq (Hz)	Freq (Hz)	Diff (%)	MAC	Freq (Hz)	Diff (%)	MAC
(1 1)	1	225	242.7	8.0%	1.00	225.4	0.3%	1.00
(0 2)	2	319	342.0	7.2%	0.99	317.5	-0.5%	0.99
(2 0)	3	423	456.3	7.8%	1.00	423.9	0.1%	1.00
(1 2)	4	561	605.1	7.9%	0.99	562.3	0.3%	0.99
(2 1)	5	602	649.0	7.9%	1.00	603.4	0.3%	1.00
(0 3)	6	936	1008.3	7.8%	0.99	937.0	0.2%	0.99
(2 2)	7	1062	1145.7	7.9%	0.99	1066.0	0.4%	0.99
(3 0)	8	1134	1218.7	7.5%	0.65	1134.1	0.0%	0.65
(3 1)	9	1332	1432.3	7.5%	1.00	1333.1	0.1%	1.00
(2 3)	10	1720	1846.2	7.4%	0.99	1719.7	0.0%	0.99
(3 2)	11	1804	1937.2	7.4%	0.94	1804.9	0.1%	0.94
(1 4)	12	2048	2190.8	7.0%	0.98	2040.3	-0.4%	0.98
(4 0)	13	2214	2372.1	7.2%	0.94	2211.2	-0.1%	0.94
(4 1)	14	2368	2536.7	7.1%	0.97	2365.5	-0.1%	0.97
(3 3)	15	2534	2723.0	7.5%	0.97	2539.8	0.2%	0.97
(2 4)	16	2605	2795.7	7.3%	0.95	2607.1	0.1%	0.95
(4 2)	17	2881	3092.9	7.4%	0.91	2886.5	0.2%	0.91
(3 4)	18	3450	3707.6	7.5%	0.86	3462.3	0.4%	0.86
(4 3)	19	3592	3858.3	7.4%	0.80	3604.3	0.3%	0.81
			μ =	**7.5%**	**0.94**		**0.2%**	**0.94**
			max =	**8.0%**			**0.4%**	

Figure 21: Comparison between model and modal tests with accelerometers before and after the adjustment process: left) driven set (4 mm); right) benchmarking set (6 mm)

As can be seen, the percentage of variation of the value of the parameters is not important (between 3% and 7%), but the effects of these variations are quite important, as shown in Fig. 21, where can be seen that the total error drops from an average of 9.7% to only 0.6%, and a maximum of 11.8% to 2.2%, in the case of the driven set of plates, and from an average of 7.5% to 0.2%, and a maximum of 8.0% to 0.4%, in the case of the benchmarking set. The MAC values, as expected, did not change.

On the other hand, when comparing the variation of the values of the parameters between the two set of plates, tendency is the same in the case of the density and lamina thickness, also with quite similar variations. This is not the case of the Young modulus in the direction of the fibers. However, this variation is lower and have a reduced impact in the final dynamic behaviour of the plates.

5.2. Model updating using results from 3D DIC measurements

As seen in section 2, even though using 3D DIC a lower number of modes are identified (twelve in the case of the driven set and seven for the benchmarking set), natural frequencies of those modes are very similar to those obtained through more classic experimental modal analysis based on direct acceleration measurements, and again high values of the MAC are computed when comparing modes shape with those numerically obtained from the theoretical FEM model. Thus, in this case the similar discrepancies between the corresponding natural frequencies have been encountered, as shown in Fig. 15. This makes it meaningful to try to apply the same methodology for model updating but based on the results of modal analysis obtained from 3D DIC. The main question was if using a much lower number of modes for updating, it was possible to obtain: i) a calibrated model with a similar degree of correlation; ii) similar values for updated parameters.

Table 7 shows the updated values obtained after model updating based on modal results from 3D DIC. In this case the variations for the two set of plates are almost exact. On the other hand, updated values of the parameters are very similar to those obtained when using modal results from accelerometers measurements for model updating, repeating the same tendency of increase of the density, decrease of the lamina thickness, and more reduced variation of the Young modulus in the direction of the fibres.

Natural frequencies obtained with those calibrated models are again very well correlated with experimental results, as shown in Fig. 22 , where can be seen that the total error drops from an average of 8.4% to only 0.46%, and a maximum of 9.1% to 1.4%, in the case of the driven set (4 mm) of plates,

Table 7: Updated values of the parameters through model updating using results from 3D DIC

Parameter	Initial value	Driven Set		Benchmarking set	
		Adjusted value	Δ	Adjusted value	Δ
E1 (GPa)	139	136	-2%	136	-2%
Density(Kg/m3)	1580	1620	2%	1617	2%
Lamina thickness (mm)	0.190	0.179	-6%	0.180	-5%

	Test		Initial FEM (f_1)			Updated FEM (f_1)		
Type	Nº	Freq (Hz)	Freq (Hz)	Diff (%)	MAC	Freq (Hz)	Diff (%)	MAC
(1 1)	1	160	173.9	8.5%	1.00	160.1	-0.1%	1.00
(0 2)	2	208	222.3	7.0%	0.99	204.7	-1.4%	0.99
(2 0)	3	282	306.1	8.5%	1.00	281.6	-0.2%	1.00
(1 2)	4	390	422.6	8.4%	0.98	389.3	-0.1%	0.98
(2 1)	5	411	447.0	8.7%	0.99	411.7	0.1%	0.99
(0 3)	6	629	677.3	7.7%	0.99	623.9	-0.8%	0.99
(3 0)	7	734	799.9	9.0%	0.76	736.4	0.4%	0.76
(2 2)	8	738	803.6	8.9%	0.96	740.6	0.4%	0.96
(1 3)	9	763	822.7	7.8%	0.86	758.4	-0.6%	0.86
(3 1)	10	894	975.3	9.1%	0.95	898.4	0.5%	0.95
(2 3)	11	1187	1287.6	8.4%	0.85	1187.4	0.0%	0.85
(3 2)	12	1228	1336.5	8.9%	0.90	1232.4	0.4%	0.90
			μ =	8.4%	0.93		0.4%	0.93
			max =	9.1%			1.4%	

	Test		Initial FEM (f_1)			Updated FEM (f_1)		
Type	Nº	Freq (Hz)	Freq (Hz)	Diff (%)	MAC	Freq (Hz)	Diff (%)	MAC
(1 1)	1	232	249.2	7.4%	1.00	232.3	0.1%	1.00
(0 2)	2	321	342.9	6.7%	0.99	319.5	-0.6%	0.99
(2 0)	3	433	465.0	7.3%	1.00	433.0	-0.1%	1.00
(1 2)	4	573	615.2	7.3%	0.98	573.8	0.1%	0.98
(2 1)	5	615	659.6	7.3%	0.99	615.0	0.1%	0.99
(0 3)	6	947	1014.4	7.1%	0.95	946.0	-0.1%	0.95
(2 2)	7	1081	1160.8	7.3%	0.87	1083.5	0.2%	0.87
			μ =	7.2%	0.97		0.2%	0.97
			max =	7.4%			0.6%	

Figure 22: Comparison between model and modal tests with 3D DIC before and after the adjustment process: left) driven set (4 mm); right) benchmarking set (6 mm)

and from an average of 7.2% to 0.2%, and a maximum of 7.4% to 0.6%, in the case of the benchmarking set (6 mm).

5.3. Final reference FEM model

Finally, the natural frequencies are calculated in the calibrated model of the plate, eliminating the mass of the accelerometer. The results are shown in Table 8. As can be observed, models updated based on DIC or accelerometer measurements are very similar. This indicates that, although a more reduced number of modes has been identified using DIC, this limitation does not necessarily mean a big restriction for the improvement of the models.

Table 8: Comparison between model and modal tests with 3D DIC before and after the adjustment process

	Driven set (4 mm)				Benchmarking set (6 mm)		
Type	**Frec (Hz)***	**Frec (Hz)****	**Dif (%)**	**Type**	**Frec (Hz)***	**Frec (Hz)****	**Dif (%)**
(1 1)	158,5	160,1	-0,99%	(1 1)	231,6	232,3	-0,27%
(0 2)	202,7	204,7	-1,00%	(0 2)	318,4	319,5	-0,35%
(2 0)	278,8	281,6	-1,01%	(2 0)	432,2	433,0	-0,17%
(1 2)	385,5	389,3	-0,99%	(1 2)	572,1	573,8	-0,30%
(2 1)	407,6	411,7	-0,99%	(2 1)	613,5	615,0	-0,25%
(0 3)	617,7	623,9	-1,00%	(0 3)	942,9	946,0	-0,32%
(3 0)	729,1	736,4	-1,00%	(2 2)	1080,6	1083,5	-0,27%
(2 2)	733,3	740,6	-0,99%	(1 3)	1130,8	1134,4	-0,32%
(1 3)	751,0	758,4	-0,99%	(3 0)	1138,4	1140,4	-0,17%
(3 1)	889,6	898,4	-0,99%	(3 1)	1349,6	1352,5	-0,21%
(2 3)	1175,8	1187,4	-0,98%	(2 3)	1729,2	1734,3	-0,29%
(0 4)	1199,7	1211,6	-0,99%	(3 2)	1812,8	1817,5	-0,26%
(3 2)	1220,4	1232,4	-0,98%	(0 4)	1824,0	1830,1	-0,34%
(1 4)	1368,1	1381,6	-0,99%	(1 4)	2047,8	2054,4	-0,32%
(4 0)	1432,2	1446,4	-0,99%	(4 0)	2213,2	2217,4	-0,19%
(4 1)	1551,5	1566,8	-0,99%	(4 1)	2371,1	2376,2	-0,21%
(3 3)	1740,0	1757,0	-0,98%	(3 3)	2548,7	2555,7	-0,27%
(2 4)	1774,2	1791,6	-0,98%	(2 4)	2610,3	2618,2	-0,30%
(4 2)	1943,8	1962,8	-0,98%	(4 2)	2893,2	2900,0	-0,24%
(0 5)	1996,5	2016,3	-0,99%	(0 5)	3005,2	3015,5	-0,34%
(1 5)	2118,7	2139,5	-0,98%	(1 5)	3170,5	3181,4	-0,34%
(5 0)	2340,3	2363,2	-0,98%	(3 4)	3467,0	3477,1	-0,29%
(3 4)	2406,1	2429,5	-0,97%	(4 3)	3607,7	3617,0	-0,26%
(4 3)	2466,5	2490,4	-0,97%	(5 0)	3619,8	3628,1	-0,23%
(5 1)	2478,9	2503,1	-0,98%	(5 1)	3759,1	3767,5	-0,22%
(2 5)	2578,6	2603,7	-0,97%	(2 5)	3781,9	3793,9	-0,32%
(5 2)	2833,3	2860,8	-0,97%	(5 2)	4222,4	4232,8	-0,25%
(0 6)	2969,2	2998,4	-0,98%	(0 6)	4426,3	4442,0	-0,35%
(1 6)	3112,5	3143,0	-0,98%	(4 4)	4591,5	4604,9	-0,29%
(4 4)	3166,2	3196,6	-0,96%	(1 6)	4614,4	4630,5	-0,35%

* Model updating using accelerometer measurements

** Model updating using 3D DIC measurements

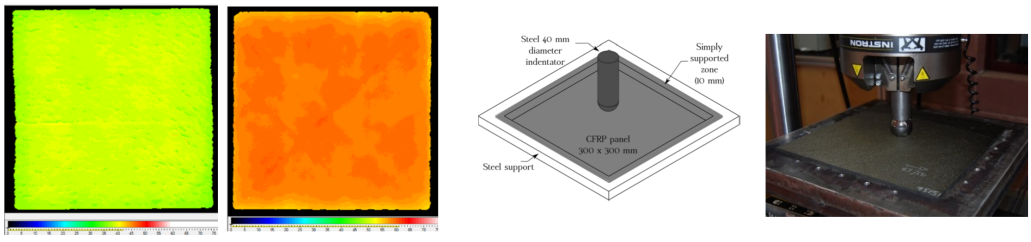

Figure 23: Left) thickness measured by ultrasonic inspection of one of driven set plates (left) and benchmarking set (right); right) overall stiffness measured by QSI test

6. Experimental validation of updated properties

To obtain a validation of model updating, experimental verification of some of the adjusted parameters was done. A detailed explanation of the experimental methods that have been used for measuring the properties of composite plates is included in reference [18], in which previous work of the authors is presented. The parameters measured are:

- total weight of the plates, verified through a high precision balance
- mean thickness, verified through ultrasonic inspection (Fig. 23 left)
- overall stiffness, verified through QSI test (Fig. 23 right)

The summary of results of this verification and comparison with updated values is shown in Fig. 24. As can be seen, the optimized values using both methods (accelerometer measurements and DIC) are much more adjusted to the measured values than the initial theoretical ones, showing a similar degree of correlation in most of the cases. Only the stiffness value updated for the driven set of plates through DIC methods is clearly more correlated than the one obtained through accelerometer measurements.

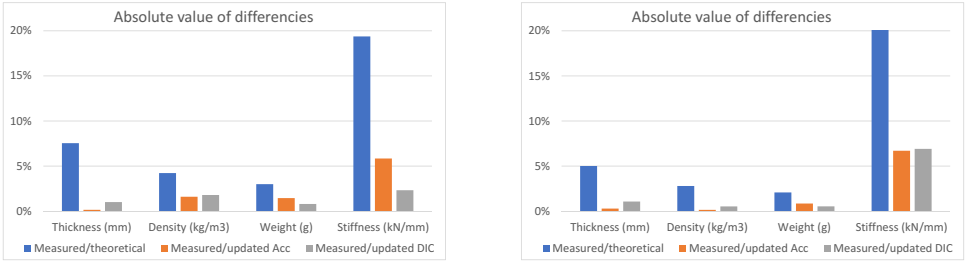

(a) Driven set (4 mm) (b) Benchmarking set (6 mm)

Figure 24: Comparison of differences between measured and theoretical, and measured and updated values of the parameters

7. Conclusions

This work presents the use of high-speed digital image correlation in experimental modal analysis compared with a more traditional form of vibration measurement based on the use of contacting sensors, such as accelerometers. Both experimental methods have been applied to modal identification in two sets of carbon/epoxy composite plates. It has been stated that, despite its capabilities, high-speed 3D-DIC vibration measurement also presents drawbacks. Full-field displacement time series measured by the camera are very noisy, due to the displacements being so small. Thus, DIC is less efficient to analyse high frequency vibrations, which involve lower amplitudes. Using the more precise accelerometer measurements and MISO techniques, it is possible to identify up to around 20 modes on the plates, whereas by using camera measurements and a SIMO method, only the first seven to twelve first modes were identified, being the rest of the modes below the noise floor.

Then, the first more traditional technique would be the clear winner. However, it must be pointed out that mode shapes obtained from 3D DIC, not only have a higher definition, because it is possible to obtain modal displacement in a much denser grid of points, but are also smoother, at least in the case of the modes of lower frequencies. These results look very promising to be applied to the localization of damage in that kind of plates. On the other hand, an additional advantage of the SIMO method lies in a significant reduction in required experimental time compared to MISO techniques, which could be crucial in some engineering applications for maintenance and Structural Health Monitoring. Subsequently, the modal parameters obtained by those experimental modal processes are used for the updating of finite element models to increase its agreement with experiments. The models of the two sets of plates were considerably improved by modifying some of their mechanical parameters (density, thickness and elastic modulus in the direction of the fibres). The effects of these updating of the parameters are quite important. The total error in natural frequencies between model and experimental results drops from average values near 10% (between 7.2% and 9.7%) to values lower than 1% (between 0.2% and 0.6%). A very important conclusion is that the degree of improvement of the models was equal, based on DIC or accelerometer measurement. Thus, the reduced number of identified modes obtained with the first experimental method seems not to represent a major limitation for this purpose. The obtained reference numerical models, physically more correct, establish the baseline of the dynamic behaviour of the carbon/epoxy composite plates, and can be applied for condition assessment or quality manufacturing control of existing structures through a

non-destructive Structural Health Monitoring, that eventually could detect degradation or defects of the composite components. Finally, the consistency of the adjusted parameters during model updating has been experimentally verified by measuring the real weight of the plates, their thickness and stiffness.

Acknowledgements

This research was done with the financial support of the Spanish Ministry of Economy and Competitiveness under Project reference DPI2013-41094-R, and the Vicerrectorado de Política Científica UC3M (Projects 2014/00006/002 and 2013/00413/003).

References

[1] M. Chandrashekhar, R. Ganguli, Damage assessment of composite plate structures with material and measurement uncertainty, Mech. Syst. Signal Pr. 75 (2016) 75–93.

[2] A. Teughels, J. Maeck, D. De Roeck, A finite element model updating method using experimental modal parameters applied on a railway bridge, Proceedings of 7th International Conference on Computer Aided Optimum Design of Structures, Bologna, 2001.

[3] A. Esfandiari, F. Bakhtiari-Nejad, M. Sanayei, A. Rahai, Structural finite element model updating using transfer function data, Comput. Struct. 88 (1) (2010) 54–64.

[4] W. Visser, Updating structural dynamics models using frequency response data, Ph.D. thesis, Department of Mechanical Engineering, Imperial College of Science, Technology and Medicine, London SW7 (1992).

[5] A. K. Mishra, S. Chakraborty, Development of a finite element model updating technique for estimation of constituent level elastic parameters of FRP plates, Appl. Math. Comput. 258 (2015) 84–94.

[6] A. K. Mishra, S. Chakraborty, Inverse detection of constituent level elastic parameters of FRP composite panels with elastic boundaries using finite element model updating, Ocean Eng. 111 (2016) 358–368.

[7] K. Sepahvand, S. Marburg, Identification of composite uncertain material parameters from experimental modal data, Probabilistic Eng. Mech. 37 (2014) 148–153.

[8] G. Petrone, V. Meruane, Mechanical properties updating of a non-uniform natural fibre composite panel by means of a parallel genetic algorithm, Compos. Part A: Appl. S. 94 (2017) 226–233.

[9] D. Moreno, B. Barrientos, C Perez-Lopez, F. Mendoza-Santoyo, Modal vibration analysis of a metal plate by using a laser vibrometer and the POD method. Journal of Optics A: Pure and Applied Optics Vol 7, 2005 Pages S356

[10] Reu, P., Rohe, D., Jacobs, L. (2017). Comparison of DIC and LDV for practical vibration and modal measurements. Mechanical Systems and Signal Processing, 86, 2-16.

[11] F. Trebuña, M. Hagara, Experimental modal analysis performed by high-speed digital image correlation system. Measurement 50, 78 - 85 (2014)

[12] Huñady, R., Hagara, M. (2017). A new procedure of modal parameter estimation for high-speed digital image correlation. Mechanical Systems and Signal Processing, 93, 66-79.

[13] Weizhuo Wang, John E. Mottershead, Alexander Ihle, Thorsten Siebert, Hans Reinhard Schubach, Finite element model updating from full-field vibration measurement using digital image correlation, Journal of Sound and Vibration, Volume 330, Issue 8, 2011, Pages 1599-1620

[14] A. J. Molina-Viedma Luis Felipe-Sesé, Elías López-Alba, Francisco A. Díaz, Comparative of conventional and alternative Digital Image Correlation techniques for 3D modal characterisation, Measurement, Volume 151, 2020, 107101

[15] Jaka Javh, Janko Slavik, Miha Boltežar, High frequency modal identification on noisy high-speed camera data, Mechanical Systems and Signal Processing, Volume 98, 2018, Pages 344-351, ISSN 0888-3270

[16] A.J. Molina-Viedma, L. Felipe-Sesé, E. López-Alba, F. Díaz, High frequency mode shapes characterisation using Digital Image Correlation and phase-based motion magnification, Mechanical Systems and Signal Processing, Volume 102, 2018, Pages 245-261, ISSN 0888-3270

[17] Reynders, E., Schevenels, M. , De Roeck, G. (2014). MACEC 3.3: A

Matlab toolbox for experimental and operational modal analysis. User manual - Report BWM-2014-06.

[18] Cuadrado, M., J.A. Artero-Guerrero, J. Pernas-Sánchez, and D. Varas. Model updating of uncertain parameters of carbon/epoxy composite plates from experimental modal data. Journal of Sound and Vibration 455 (2019): 380-401.

[19] International Digital Image Correlation Society, Jones, E.M.C. and Iadicola, M.A. (Eds.) (2018). A Good Practices Guide for Digital Image Correlation. DOI: 10.32720/idics/gpg.ed1

[20] Reu, P. All about speckles: Speckle Size Measurement. Exp Techniques, 38: 1-2. (2014), doi:10.1111/ext.12110.

[21] Hunter, J. D., Matplotlib: A 2D graphics environment, Computing in Science&Engineering,Volume 9, Number 3, Pages 90-95, 2007. Doi: 10.1109/MCSE.2007.55

[22] R. Allemagne, The Modal Assurance Criterion (MAC)-twenty years of use and abuse. Sounds and Vibration (2003) 14–21.

[23] E. Reynders, R. Pintelon, G. De Roeck, Uncertainty bounds on modal parameters obtained from stochastic subspace identification. Mechanical Systems and Signal Processing 2008, volume 22, number 4, Pages 948–969.

[24] P. Qiao, K. Lu, W. Lestari, J. Wang, Curvature mode shape-based damage detection in composite laminated plates, Composite Structures, Volume 80, Issue 3, 2007, Pages 409-428.

[25] M.K. Yoon, D. Heider, J.W. Gillespie, C.P. Ratcliffe, R.M. Crane, Local damage detection using the two-dimensional gapped smoothing method, Journal of Sound and Vibration, Volume 279, Issues 1-2, 2005, Pages 119-139.

[26] S. Rucevskis, M. A. Sumbatyan, P. Akishin, A. Chate, Tikhonov's regularization approach in mode shape curvature analysis applied to damage detection, Mechanics Research Communications, Volume 65, 2015, Pages 9-16.

[27] T. Marwala, Finite Element Model Updating Using Computational Intelligence Techniques, Springer Verlag, London, 2010.

[28] M. Friswell, J.E. Mottershead, Finite element model updating in structural dynamics, Springer Science & Business Media 38 (2013).

[29] Ansys, User's manual, ANSYS Release 18.1 (2017).

[30] M. Cuadrado, E. Moliner. Modeling and long term structural health monitoring of Villanueva del Jalón viaduct, Eurodyn 2014, IX International Conference on Structural Dynamics, Porto, 2014.

[31] E. Moliner, M. Cuadrado, Assessment of Long-Term Structural Health at Villanueva del Jalón Viaduct, Proceedings of the Second International Conference on Railway Technology: Research, Development and Maintenance, Civil-Comp Proceedings, 2014.

[32] D. Ribeiro, R. Calçada, R. Delgado, M. Brehm, V. Zabel, Finite element model updating of a bowstring-arch railway bridge based on experimental modal parameters, Eng. Struct. 40 (2012) 413–435.